Quantum phase transition of nonlocal Ising chain with transverse field in a resonator

Yu-Na Zhang, Xi-Wang Luo, Guang-Can Guo, Zheng-Wei Zhou,* and Xingxiang Zhou†

Key Laboratory of Quantum Information, University of Science and Technology of China, Hefei, Anhui 230026, People's Republic of China and Synergetic Innovation Center of Quantum Information and Quantum Physics, University of Science and Technology of China, Hefei, Anhui 230026, People's Republic of China

(Received 8 April 2014; revised manuscript received 22 August 2014; published 15 September 2014)

We study the quantum phase transition in a spin chain with variable Ising interactions and position-dependent coupling to a resonator field. Such a complicated model, usually not present in natural physical systems, can be simulated by an array of qubits based on man-made devices and exhibits interesting behavior. We show that, when the coupling between the qubit and field is strong enough, a superradiant phase transition occurs, and it is possible to pick a particular field mode to undergo this phase transition by properly modulating the strength of the Ising interaction. We also study the impact of the resonator field on the magnetic properties of the spin chain and find a rich set of phases characterized by distinctive qubit correlation functions.

DOI: 10.1103/PhysRevB.90.094510 PACS number(s): 03.67.Ac, 75.10.−b, 85.25.Cp

I. INTRODUCTION

Quantum simulation is a powerful tool to study difficult physics problems that cannot be easily solved analytically or simulated with a classical computer [1–6]. In order to study such hard problems, the simulation system must be carefully designed and set up to capture as much as possible the essence of the simulated problem. This requirement often poses a great challenge and can only be met to a certain degree. It is one of the main reasons why many quantum simulation protocols are very difficult to realize experimentally. This issue is especially prominent in simulation systems based on artificial atoms such as Josephson devices, because many of their properties are fundamentally different than those of natural physical particles [7–11].

Although the inevitable discrepancy between the simulation and simulated systems is often considered an obstacle in quantum simulation, it can also provide opportunities for studying physics models under conditions not easily accessible in natural physical systems. This is because, due to the excellent controllability available in simulation systems based on man-made devices, one can often tune the critical physical parameters over a range far greater than what is feasible in a natural physical system and even realize configurations not possible in a natural physical system. To explore such opportunities in quantum simulation that have not received sufficient attention, we study the quantum phase transitions in a nonlocal Ising chain interacting with a resonator. This problem has its root in the well-known Dicke model [12–14], in which a collection of identical and noninteracting two-level atoms are coupled to a single electromagnetic (EM) field mode. Our problem has a few important differences from the original Dicke model, in that many qubits are spread out within a single wavelength of a multimode EM field, and there are controllable interactions between the qubits. It is also possible to tune the transverse field of each qubit individually. These characteristics, usually not present in a natural atom-cavity system, are accessible in simulation systems based on artificial atoms and man-made devices, and they have profound impact on the behavior of the system and the method we use to treat it.

A possible physical realization of our simulation model is depicted in Fig. 1. It consists of N superconducting charge qubits placed at equal distances and capacitively coupled to a transmission-line resonator (TLR). The charge qubit is biased at the charge degeneracy point to make it an effective two-level system. The TLR supports multiple resonant modes that the charge qubits interact with [15–17]. This simulation system is analogous to an atom-cavity system in the Dicke model, but with notable differences. In a natural atom-cavity system, because the size of an atom is so small, the displacement between individual atoms in an atomic cloud is negligible compared with the wavelength of the EM field, and we can use the "long-wavelength approximation" which assumes that the atoms are at the same location and their coupling strengths to the EM field are identical. This approximation does not apply in the system in Fig. 1 because the charge qubits, being macroscopic devices much larger than atoms, can spread out along the entire TLR length which is also the wavelength (or its multiple) of the EM modes that they couple to, and the position dependence of the coupling strength must be taken into account. Another important distinction concerns the fact that it is difficult to induce significant interactions between charge-neutral atoms. This limitation can be overcome in our system by introducing coupling circuitry as shown in Fig. 1. By using large Josephson junctions inductively coupled to the charge qubits, we can induce strong and adjustable interactions between them, greatly enriching the physics of our system.

In the following, we focus on phase transitions in our system of spatially separated and interacting qubits coupled to a resonator field with multiple modes. In the traditional Dicke model, the atom-field coupled system is subject to an instability due to the interaction between the atom and field. When the interaction strength grows above a critical value, the field of the ground state of the system is no longer in the vacuum mode. It becomes macroscopically occupied with photons and the system enters the so-called superradiant phase [18]. In our system, we find that the superradiant phase transition can also occur when the coupling strength between the qubits and the resonator field is strong enough, although

*zwzhou@ustc.edu.cn
†xizhou@ustc.edu.cn

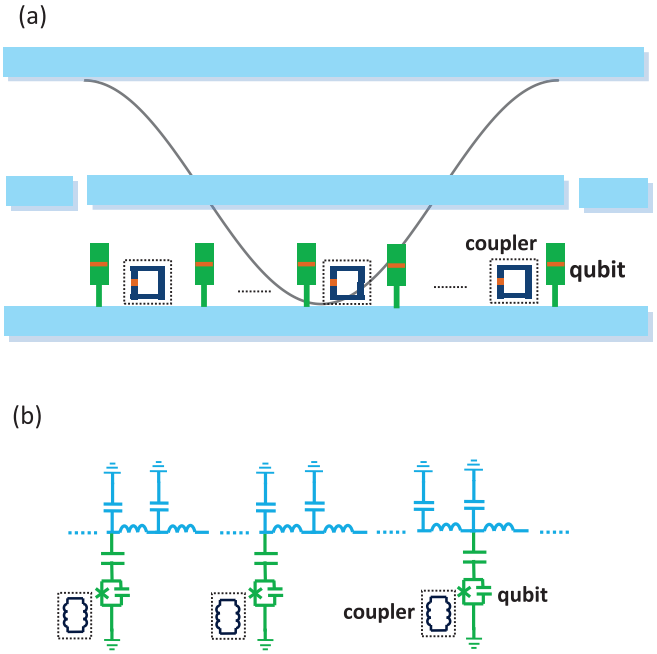

FIG. 1. (Color online) (a) An array of charge qubits capacitively coupled to the TLR. The TLR consists of a center conductor and two ground planes. The voltage between the center conductor and the ground planes is position dependent, as indicated by the cosine curve in the figure. The charge qubits located between the center conductor and ground plane are capacitively coupled to the center conductor. The nearest-neighbor interaction between charge qubits is realized by an rf superconducting quantum interference device (in the dashed box). (b) The equivalent distributed circuit of panel (a).

the details of the phase transition is much more complicated. Furthermore, by periodically modulating the strength of the interaction between the qubits, we can select which mode of the resonator field undergoes the superradiant phase transition. We then study the magnetic properties of the qubit chain and its phase transitions which are impacted by the state of the resonator field.

II. MODEL HAMILTONIAN

The full Hamiltonian of our system reads

$$H = H_Q + H_R + H_{R\text{-}R} + H_{Q\text{-}R} + H_{Q\text{-}Q}. \tag{1}$$

Among these terms, the Hamiltonian of the N-qubit system

$$H_Q = -\frac{E_z}{2}\sum_{j=0}^{N-1}\sigma_j^z \tag{2}$$

is written in the eigenbasis $\{(|0\rangle \pm |1\rangle)/\sqrt{2}\}$ at the charge-degeneracy point, with $|0\rangle$ and $|1\rangle$ the 0 and 1 excess charge state. The multimode (labeled by the energy quantum number l) resonator field Hamiltonian is

$$H_R = \sum_l \omega_l b_l^\dagger b_l. \tag{3}$$

The coupling between the qubit system and the resonator field is assumed to be dipolar and described by

$$H_{Q\text{-}R} = -\sum_j\sum_l \frac{\lambda_l(j)}{\sqrt{N}}\sigma_j^x(b_l^\dagger + b_l), \tag{4}$$

where the coupling strength

$$\lambda_l(j) = \lambda_0\sqrt{l}\cos(l\pi j/N) \tag{5}$$

is dependent on the position of the qubits which are assumed to be equally spaced. In addition, we also have terms for the self-energy of the resonator field and nearest-neighbor qubit interaction,

$$H_{R\text{-}R} = \sum_l D_l(b_l + b_l^\dagger)^2 \tag{6}$$

and

$$H_{Q\text{-}Q} = -\sum_j J(j)\sigma_j^y\sigma_{j+1}^y. \tag{7}$$

Here, D_l is the field self-interaction strength and the $J(j)$s characterize the position-dependent Ising interaction strength.

The Hamiltonian in Eq. (1) has several important differences from the conventional Dicke model:

(1) The EM field can have multiple modes, consistent with the situation in physical resonators.

(2) The long-wave approximation does not apply and the coupling between the qubit and field is dependent on the position of the qubit.

(3) There is an Ising interaction between nearest-neighbor qubits.

These new elements in our model have a profound impact on the system behavior and phase transitions. As mentioned in the introduction, such a model Hamiltonian can be realized by using man-made devices with excellent controllability such as the charge-qubit–TLR system in Fig. 1. As shown in Appendix A, in such a system the qubit energy is equal to the Josephson energy E_z of the charge qubit. The resonator-mode frequencies are determined by the parameters of the TLR, $\omega_l = l\pi/(d\sqrt{L_0C_0})$, where L_0 and C_0 are the inductance and capacitance per unit length of the TLR and d is its length. The qubit-field coupling strength $\lambda_0 = \frac{eC_g}{C_\Sigma}\sqrt{\frac{N\omega_1}{dC_0}}$, where C_g and C_Σ are the gate capacitance of the charge qubit and the total capacitance of the charge island, respectively, and the field self-interaction strength $D_l = \frac{1}{N}\sum_j \frac{C_\Sigma}{2e^2}\lambda_l^2(j)$.

III. QUANTUM PHASE TRANSITION

A. Mean-field treatment

The solution of our system is complicated by the fact that the resonator field has multiple modes. To avoid nonessential complications and focus on the study of phase transitions, we will adjust the system parameters such that no more than one resonator mode has macroscopic occupation. To find the conditions for such a setup, we consider one resonator mode l first and use the mean-field approximation to simplify the

qubit-resonator coupling term $H_{Q\text{-}R}$ as

$$\sum_j \frac{\lambda_l(j)}{\sqrt{N}}(b_l^\dagger + b_l)\sigma_j^x = \sum_j 2\phi_l\lambda_l(j)\sigma_j^x + \sqrt{N}(b_l^\dagger + b_l)\Sigma_l^x - 2N\phi_l\Sigma_l^x, \quad (8)$$

where the order parameters

$$\phi_l = \langle G|\frac{(b_l^\dagger + b_l)}{2\sqrt{N}}|G\rangle,$$
$$\Sigma_l^x = \langle G|\frac{\sum_j \lambda_l(j)\sigma_j^x}{N}|G\rangle, \quad (9)$$

with the ground state of the system being $|G\rangle$.

Under the mean-field approximation, the qubit part of the Hamiltonian becomes that of a nonlocal Ising chain with a transverse field dependent on ϕ_l, which is the order parameter for the resonator field. As shown in Appendix B, it can be solved by the Jordan–Wigner transformation which maps the Ising chain to a collection of fermionic quasiparticles. The energy per particle for the system is

$$e_g = \left(\omega_l\phi_l^2 + 4D_l\phi_l^2 - \frac{1}{2N}\sum_k \Lambda_k(\phi_l)\right), \quad (10)$$

where the spectrum of the quasiparticles Λ_k is a complicated function dependent on ϕ_l, as shown in Appendix B. By finding the value of ϕ_l that minimizes e_g, we can determine the ground-state energy and the order parameter ϕ_l^g for the resonator field. Unlike in conventional Dicke problems, this problem cannot be solved analytically because of the complicated quasiparticle spectrum Λ_k. Thus we numerically solve for ϕ_l^g, which is the order parameter of the resonator field for the ground state.

B. Superradiant phase transition

In this section, we focus on the state of the resonator field. We start with the simple case of the homogeneous Ising interaction $J(j) = J, \forall\, j$, and calculate the ground-state-field order parameter ϕ_l^g for different values of qubit-field coupling strength λ_0 and Ising interaction strength J. In Figs. 2(a) and 2(b), the numerical results of ϕ_l^g for $J = 0.05$ and $J = 0.35$ (in units of ω_1) are shown. It is seen that, when the qubit-field coupling λ_0 is small, the ground-state energy is minimized when $\phi_l^g = 0$. When λ_0 is greater than a critical value λ_0^c, ϕ_l^g becomes nonzero, indicating that the photon field has a macroscopic occupation. Therefore, a superradiant phase transition occurs when the qubit-field coupling becomes strong enough.

We also calculated ϕ_l^g for different resonator modes l. We find that, for homogeneous Ising interaction $J(j) = J$, the critical points λ_0^c for all resonator modes are the same. Therefore, when λ_0 increases, all the resonator modes undergo the superradiant transition at the same critical point λ_0^c. In Figs. 2(a) and 2(b), the results are obtained by considering only one mode in the calculation as shown in Sec. III A. Since the plots indicate that all resonator-field modes can become macroscopically occupied at the same time, a more rigorous treatment requires including all resonator modes in the calculation. This is challenging numerically since the amount of calculation required increases dramatically with the number of resonator modes included. In Fig. 2(c), the results are plotted when the first three resonator modes are considered simultaneously. We see that, the average values for all resonator-field modes indeed become nonzero at the same critical point, consistent with the results in Fig. 2(a).

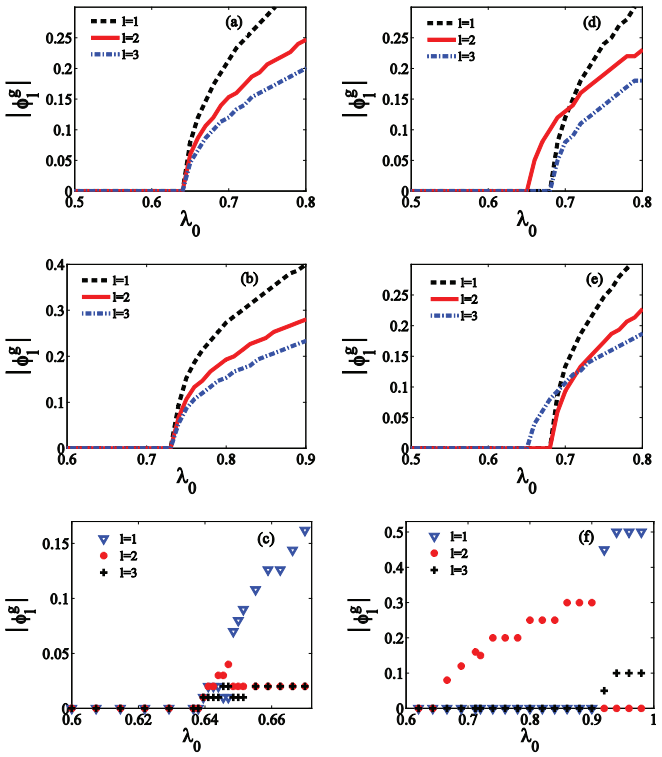

FIG. 2. (Color online) ϕ_l^g versus λ_0 for different resonator modes l. In panels (a) and (b), only one mode is considered in the calculation, although a different mode is used for each curve. The Ising interaction is homogeneous, $J(j) = J$, and $J = 0.05$ and 0.35, respectively. In panel (c), the ground-state values of three modes ($l = 1,2,3$) are plotted for a homogeneous Ising interaction $J = 0.05$ by considering all modes simultaneously in the calculation. In panels (d) and (e), $J(j)$ has a rectangular waveform as in Eqs. (11) and (12), and $J_{\max} = 0.35$, $J_{\min} = 0.05$ are used. The modes $l = 2$ and $l = 3$ are singled out since the critical value λ_0^c for them to undergo the superradiant transition is the lowest. Only one mode is considered in each calculation. In panel (f), three modes are considered simultaneously in the calculation. $J(j)$ has a rectangular waveform as in Eq. (11), and $J_{\max} = 0.35$, $J_{\min} = 0.05$. In panel (a)–(f), the parameters, $\frac{e^2}{2C_\Sigma} = 8$ and $E_z = 0.8$, are chosen to be accessible values in typical experiments. The size of the system is $N = 200$.

For our studies, we wish to pick a particular mode to undergo the superradiant phase transition. This can be accomplished by making the critical value λ_0^c for the chosen mode lower than that of other modes. For this purpose, we make the Ising interaction strength $J(j)$ inhomogeneous and position dependent. We find that, by giving $J(j)$ a spatial modulation as simple as a rectangular wave, we can lower the critical value λ_0^c for one particular resonator mode below that of all others. For example, if the position dependence of $J(j)$ is

$$J(j) = \begin{cases} J_{\max}, & j \in [N/8,3N/8] \text{ and } [5N/8,7N/8] \\ J_{\min} & \text{all other sites,} \end{cases} \quad (11)$$

the critical value λ_0^c for the mode $l = 2$ is the lowest, as shown in Fig. 2(d). If instead the position dependence of $J(j)$ is

$$J(j) = \begin{cases} J_{\max}, & j \in [N/12,3N/12] \text{ and } [5N/12,7N/12] \\ & \text{and } [9N/12,11N/12] \\ J_{\min} & \text{all other sites,} \end{cases} \tag{12}$$

then the mode $l = 3$ becomes the first one to undergo the superradiant phase transition when λ_0 increases, as shown in Fig. 2(e). In these examples, notice that the period of $J(j)$ is the same as that of the chosen resonator mode. Also, the gap between the critical value of λ_0^c for the chosen mode and others increases with the amplitude of the Ising-interaction-strength modulation, $\Delta J = |J_{\max} - J_{\min}|$. In Figs. 2(d) and 2(e), only one mode is included in each calculation. To check the validity of the conclusion derived from this simplification, we also performed the calculation by including all three modes simultaneously and plot the results in Fig. 2(f). It is seen that the critical value of λ_0 for the first mode to undergo the superradiant phase transition remains approximately the same as that in Fig. 2(d), and there is a clear gap in the values of λ_0 for other modes to undergo the phase transition. Therefore, by using this technique we can in principle single out a resonator mode to undergo the superradiant phase transition while all other modes remain unoccupied.

C. First- and second-order quantum phase transition

The exact nature of the quantum phase transition (QPT) of the resonator field and its relation with the Ising interaction strength $J(j)$ and transverse field E_z is an interesting topic in our problem. To study it, we first choose a single mode to undergo the superradiant phase transition while all other modes remain in the unpopulated state. Specifically, we focus on the mode $l = 2$ by modulating the Ising interaction strength as in Eq. (11). Assuming a transverse field $E_z = 0.8$, we fix the amplitude of the Ising interaction modulation by setting $\Delta J = 0.375E_z = 0.3$ and use the value of $J_{\min}$ as the measure for the strength of the Ising interaction. We then calculate the order parameter ϕ_2^g as a function of $J_{\min}$ and the qubit-field coupling strength λ_0. This will allow us to examine the phase transition in great detail and determine its exact nature. The results are plotted in Fig. 3.

We find that, when the Ising interaction is weak and the value of $J_{\min}$ is small, the transition of ϕ_2^g from 0 to a nonzero value is continuous. This smooth increase in ϕ_2^g is the most conspicuous signature for a second-order QPT which is represented by the red dashed line in Fig. 3. On the other hand, when $J_{\min}$ increases above about 0.35, the transition to a nonzero value for ϕ_2^g becomes discontinuous, indicating that the phase transition has changed to first order. This is labeled by the blue solid line. Since the first-order phase transition grows out of a second-order one, there will be a region where the jump of ϕ_2^g is small [19,20].

To demonstrate clearly the differences between the second- and first-order QPT, we consider two cases where $J_{\min}$ is much smaller and much greater than 0.35 and calculate the single-particle energy e_g as a function of ϕ_2 for different values of λ_0 near the critical point λ_0^c. This will reveal how the strength of the Ising interaction $J_{\min}$ impacts the nature of the phase

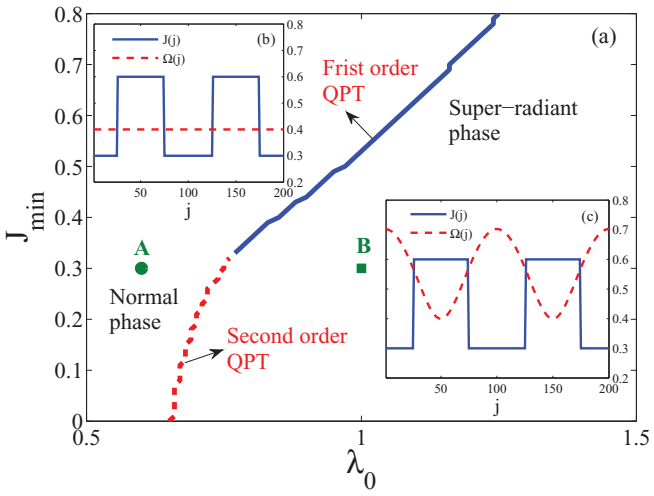

FIG. 3. (Color online) Phase diagram of the superradiant quantum phase transition (QPT) in the $J_{\min}$-λ_0 plane. When the phase transition occurs, the mean-field value ϕ_2^g changes from 0 (the normal phase) to nonzero (the superradiant phase). When $J_{\min}$ is small, the change of ϕ_2^g from 0 to nonzero is continuous. When $J_{\min}$ is greater than 0.35 (roughly), this change becomes discontinuous. Correspondingly, the phase transition changes from second order to first order. In the upper-left and lower-right corner, the Ising interaction strength $J(j)$ and effective transverse field $\Omega(j)$ at points A and B in the phase diagram are plotted. $J(j)$ is modulated as in Eq. (11) to single out the mode $l = 2$ for the superradiant phase transition. The effective transverse field $\Omega(j) = \{(\frac{E_z}{2})^2 + [2\lambda_2(j)\phi_2^g]^2\}^{1/2}$ [see Eq. (B4)] is dependent on the order parameter ϕ_2^g. At point A in the normal phase, $\phi_2^g = 0$ and $\Omega(j)$ is constant. At point B in the superradiant phase, ϕ_2^g is nonzero and $\Omega(j)$ is oscillatory because of the position dependence of λ_2, as in Eq. (5). Parameters used in the simulation are $\frac{e^2}{2C_\Sigma} = 8$, $E_z = 0.8$, $l = 2$, $N = 200$, and $\Delta J = 0.3$.

transition. The result for $J_{\min} = 0.3$ is shown in Fig. 4(a). In the curves for e_g, we see that the single minimum at zero field continuously splits into two symmetrically located minima as the field-qubit coupling λ_0 is increased. This smooth transition signals a second-order QPT. To verify this, we further calculate the first and second derivative of the ground-state energy e_{gg} with respect to the parameter λ_0 and plot the result in Figs. 4(b) and 4(c) [21,22]. It is seen that the first derivative is continuous, whereas the second derivative is discontinuous. We can then conclude that the phase transition is indeed second order in this case. In Fig. 4(d), the single-particle energy with $J_{\min} = 0.5$ is shown for different values of λ_0. In these curves, as λ_0 increases, the number of local minima in e_g changes from one to three and then to two. When the two minima at nonzero ϕ_2^g appear, the original local minimum at zero field does not vanish and remains the global minimum of the system. When λ_0 increases further, the energy at the local minima corresponding to nonzero ϕ_2^g abruptly become the global minimum. In Figs. 4(e) and 4(f), the ground-state energy and its first derivative with respect to λ_0 are plotted. Since the first derivative is discontinuous, the phase transition in this case is first order.

The reason for the QPT changing to first order is that, when the Ising interaction is strong, the qubit chain is in the

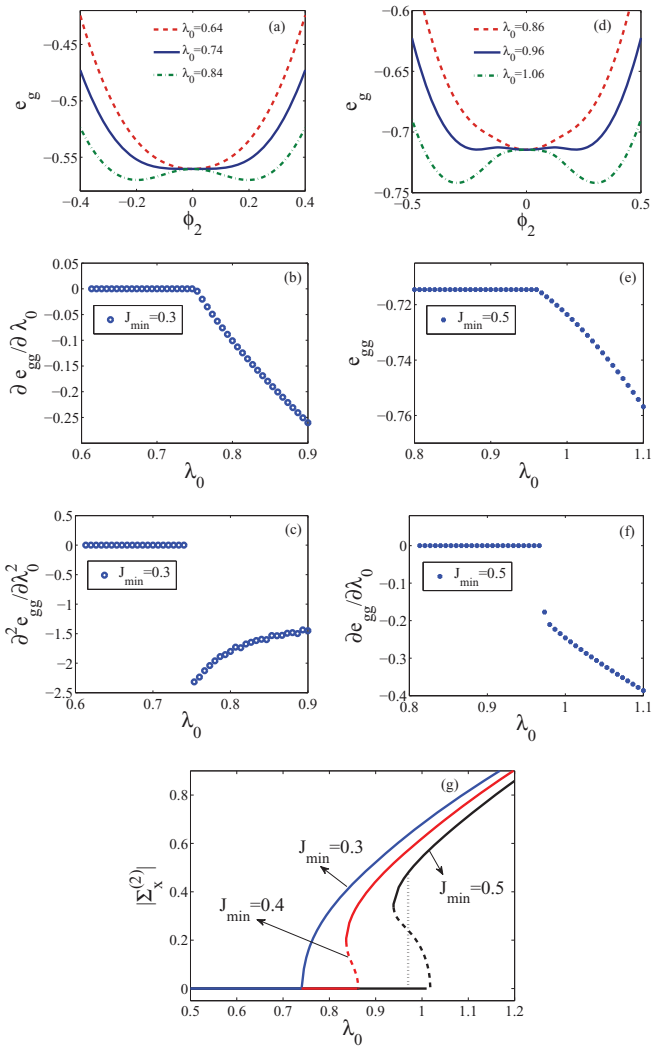

FIG. 4. (Color online) (a)–(f) The single-particle energy e_g, ground-state energy e_{gg}, and the first and second derivative of e_{gg}. In panels (a)–(c), $J_{\min} = 0.3$, and the phase transition is second order. In panels (d)–(f), $J_{\min} = 0.5$, and the phase transition is first order. Other parameters are the same as in Fig. 3. (g) $|\Sigma_2^x|$ as a function of λ_0 for different values of $J_{\min}$. The red, blue, and black solid lines refer to the values of $|\Sigma_2^x|$ for the stable points of the minimum energy in the e_g-ϕ_2 plane. The dashed lines refer to the values of $|\Sigma_2^x|$ for the unstable points of the maximum energy in the e_2-ϕ_2 plane. The vertical dotted line marks the critical point of the first order QPT for $J_{\min} = 0.5$. To the left of the dotted line, $|\Sigma_2^x| = 0$ for the ground state of the system. To the right of this line, the value of $|\Sigma_2^x|$ for the ground state becomes nonzero.

ferromagnetic phase before the superradiant phase transition occurs. Once the superradiant phase transition occurs, the qubit chain experiences a large effective transverse field due to the nonzero field value ϕ_2^g. As a consequence, the qubit chain may abruptly switch to a paramagnetic phase, which in turn leads to a discontinuous change in the first-order derivative of e_{gg}.

We can further study the nature of the phase transition by investigating the magnetic properties of the qubit chain. In Appendix B we show that, at the minima or maxima of $e_g(\phi_2)$, the order parameter for the qubit system is related to that of

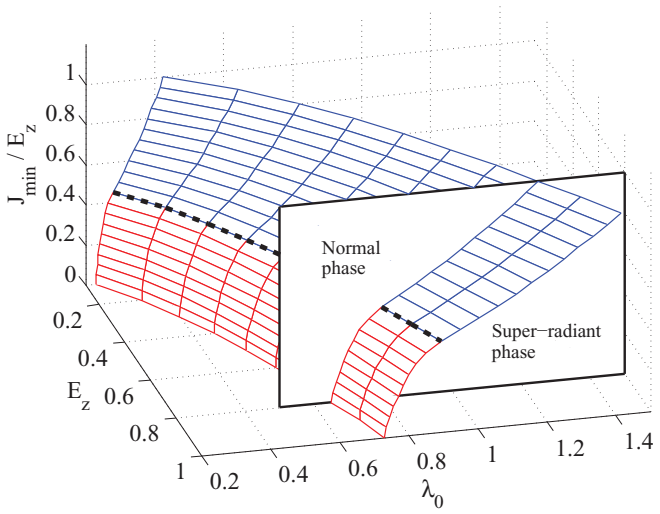

FIG. 5. (Color online) The full phase diagram in the parameter space $(E_z, \lambda_0, J_{\min})$. The $\lambda_0 - J_{\min}$ plane at $E_z = 0.8$ (which corresponds to Fig. 3) is shown, and the black dashed line marks the boundary between the first and second order phase transition. The effective transverse field is constant in the normal phase and oscillatory in the superradiant phase as in Fig. 3. Here, we set $\Delta J = 0.375 E_z$. Other parameters are the same as Fig. 3.

the field according to

$$\phi_2 = \frac{\Sigma_2^x}{\omega_2 + 4D_2}. \tag{13}$$

In Fig. 4(c), we plot $|\Sigma_2^x|$ at the minima or maxima of e_g versus λ_0. We can see that, when $J_{\min} = 0.3$, $|\Sigma_2^x|$ changes continuously with λ_0 which indicates that the QPT is second order in nature. When $J_{\min} = 0.4$ or 0.5, the curve for $|\Sigma_2^x|$ is hysteretic, suggesting that a first-order QPT takes place.

In Fig. 3, a typical value of 0.8 was used for the transverse field E_z. To study the dependence of the QPT on E_z, we calculate the phase diagram in the three-dimensional parameter space $(E_z, \lambda_0, J_{\min})$ and plot the result in Fig. 5. In this calculation, still the $l = 2$ mode is picked for the superradiant phase transition, and the modulating amplitude is fixed at $\Delta J = 0.375 E_z$. It is seen that the basic structure of the phase diagram remains the same as in Fig. 3 at different values of E_z, although the critical value of λ_0^c increases as E_z grows.

D. Magnetic orders in the ground states

The qubit part of our system is essentially a nonlocal Ising chain subject to a transverse magnetic field dependent on the state of the resonator field. In a homogeneous Ising chain (J is position independent) with uniform transverse field, the physics is dictated by the competition between the Ising interaction and the transverse field, and it is well known that the system has a critical point when the two are equally strong. In our system, this mechanism continues to play a major role. In addition, the state of the resonator field and its phase transition has a nontrivial impact on the property and behavior of the qubit chain, and we expect richer physics due to the interplay between the qubit and resonator field.

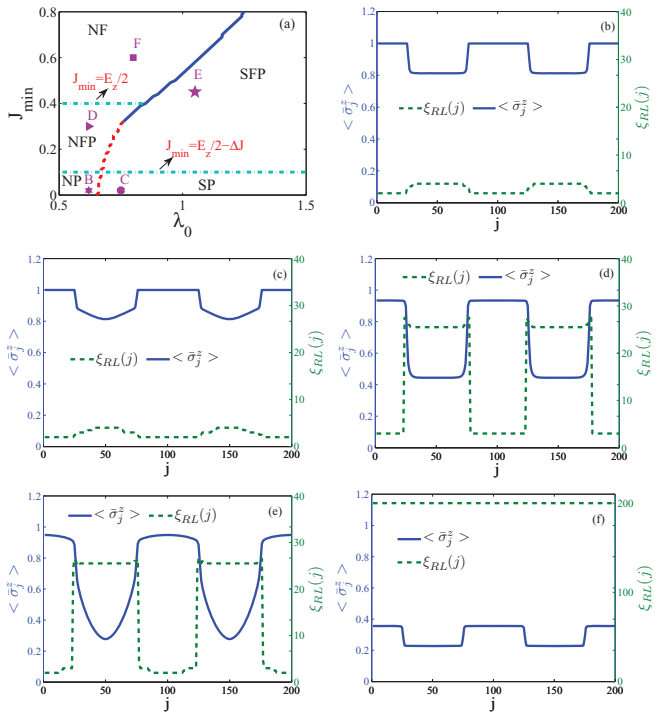

FIG. 6. (Color online) (a) Phase diagram of the system. All parameters are the same as in Fig. 3(a). (b)–(f) Values of $\langle\bar{\sigma}_j^z\rangle$ and the correlation length $\xi_{LR}(j)$ at points B–F in panel (a).

To study the properties of the qubit chain, we focus our attention on the qubit correlation $\langle\bar{\sigma}_j^y\bar{\sigma}_{j+n}^y\rangle$ [see Eq. (C1) in Appendix C], where $\bar{\sigma}_j^y$ is the Pauli matrix of the jth qubit in the direction of the Ising interaction. Since this correlation decreases with the qubit separation n, we can use it to characterize the correlation properties of the qubit chain. For the inhomogeneous Ising chain in our problem, we define $\xi_R(j)$ as the right correlation length for the jth qubit if $\langle\bar{\sigma}_j^y\bar{\sigma}_{j+\xi_R}^y\rangle = e^{-1}\langle\bar{\sigma}_j^y\bar{\sigma}_{j+1}^y\rangle$. Likewise, we define $\xi_L(j)$ as the left correlation length for the jth qubit if $\langle\bar{\sigma}_j^y\bar{\sigma}_{j-\xi_L}^y\rangle = e^{-1}\langle\bar{\sigma}_j^y\bar{\sigma}_{j-1}^y\rangle$. $\xi_{RL}(j) = [\xi_R(j) + \xi_L(j)]/2$ is the average of the left and right correlation length for the jth qubit.

In Fig. 6, we calculate and plot the mean spin $\bar{\sigma}_j^z$ and correlation length $\xi_{RL}(j)$ for a few representative points in the phase space of the system using methods developed in Appendix C. These points are selected such that they span both the normal and superradiant phase of the resonator field and cover both the weak- and strong-Ising-interaction regime. Information obtained from the plots of $\bar{\sigma}_j^z$ and $\xi_{RL}(j)$ can then help us understand the impact of the resonator field and Ising interaction on the qubit chain.

The situation when the resonator field is in the normal phase regime with $\phi_2^g = 0$ is shown in Figs. 6(b), 6(d), and 6(f). Since the resonator field is unpopulated, the transverse field is simply $E_z/2$, and the state of the qubit chain is mainly determined by its competition with the Ising interaction strength. It can be seen in Fig. 6(b) that, when the Ising interaction is weak (roughly speaking, $J_{\min} < E_z/2 - \Delta J$), the ground state of the system exhibits the normal-paramagnetic (NP) order with a large $\langle\bar{\sigma}_j^z\rangle$ and a small correlation length $\xi_{LR}(j)$. In contrast, when all local Ising interactions dominate the transverse field ($J_{\min} > E_z/2$), the qubit chain is in a normal-ferromagnetic (NF) state with a small $\langle\bar{\sigma}_j^z\rangle$ and a large correlation length $\xi_{LR}(j)$, as shown in Fig. 6(f). In between these two cases ($J_{\min} < E_z/2 < J_{\max}$), we have an interesting scenario where the transverse field and Ising interaction is dominant in different segments of the qubit chain. Consequently, both the paramagnetic and ferromagnetic orders are present in the system. This is evidenced by the oscillating behavior of $\langle\bar{\sigma}_j^z\rangle$ and $\xi_{LR}(j)$ along the qubit chain, as shown in Fig. 6(d). We call it the normal-ferromagnetic-paramagnetic (NFP) order.

When the resonator field is in the superradiant-phase regime, $\phi_2^g \neq 0$, the effective transverse field for the jth qubit is position and ϕ_2^g dependent [see Eq. (B4) in Appendix B]. If the Ising interaction is weak, $J_{\max} < E_z/2$, the local transverse field $\Omega(j)$ is always larger than $J(j)$ along the qubit chain. This leads to the superradiant-paramagnetic (SP) order with a large $\langle\bar{\sigma}_j^z\rangle$ and a small correlation length $\xi_{LR}(j)$, as shown in Fig. 6(c). As the strength of the Ising interaction increases, it is possible for the transverse field to dominate $[\Omega(j) > J(j)]$ in some segments and the Ising interaction to dominate $[J(j) > \Omega(j)]$ in the rest of the qubit chain. As shown in Fig. 6(e), the ground state of the system exhibits the superradiant-ferromagnetic-paramagnetic (SFP) order characterized by oscillating $\langle\bar{\sigma}_j^z\rangle$ and $\xi_{LR}(j)$. For the parameters we calculated, there is no superradiant-ferromagnetic (SF) order when the strength of the Ising interaction is increased further, and ϕ_2^g coexists with $\langle\bar{\sigma}_j^z\rangle$.

IV. EXPERIMENTAL CONSIDERATION

In solving the model Hamiltonian in Eq. (1) and investigating possible phase transitions in the system, we have explored a large range for the values of relevant parameters in the model. In reality, the reachable parameter space is limited by the currently available technology. For the charge-box—TLR system in Fig. 1, the TLR frequency and the Josephson energy of the charge boxes are typically around a few gigahertz. The coupling strength between a single qubit and the TLR field can range from a few kHz to nearly 1 GHz [5,23]. Since the effective coupling strength λ_0 is proportional to $\sqrt{N}$, a larger number of charge boxes placed in the TLR will result in a stronger coupling. However, the number of qubits in the charge-box array is limited by decoherence and the requirement for the two-state approximation to hold [24].

Figure 7 shows our numerical results with the following parameters: $\omega_1 \simeq 3$ GHz, the second mode frequency $\omega_2 = 2\omega_1$, $E_z = 0.1\omega_1$, $N = 40$, and $\lambda_0 \in [0, 0.25\omega_1]$. These parameters are accessible in present experiments [15,23,25]. Considering the challenge in realizing very strong Ising interaction [26], we use experimentally accessible values $J_{\max} = 0.26E_z$ and $J_{\min} = 0.01E_z$ [26,27]. As an example, we consider the case where the Ising interaction strength is modulated according to Eq. (11) and the second resonator mode undergoes the superradiant transition. Since $J(j) < 0.26E_z$ is in the weak-interaction regime, the qubit chain is restricted to the NP and SP phases. Plotted in Figs. 7(b) and 7(c) are the correlation lengths and $\langle\bar{\sigma}_j^z\rangle$ at point A (in the normal phase) and B (in the superradiant phase) in Fig. 7(a). Because of the limited Ising interaction strength, the main characteristics of these two plots are similar. To achieve the NFP and SFP phases,

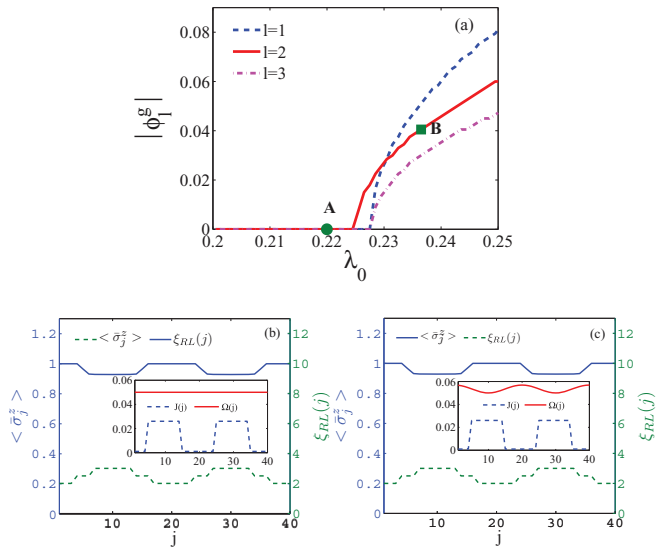

FIG. 7. (Color online) (a) $|\phi_l^g|$ versus λ_0 for different values of l with $E_z = 0.1$ (in units of ω_1), and $J_{\max} = 0.26E_z$, $J_{\min} = 0.01E_z$. In the normal phase, the order parameter $\phi_l^g = 0$. As λ_0 crosses the critical value, ϕ_l^g becomes nonzero, and the system enters superradiant phase. Panels (b) and (c) show $\langle\bar{\sigma}^z(j)\rangle$ and $\xi_{RL}(j)$ for the normal phase (point A) and superradiant phase (point B). Both are in the paramagnetic regime.

a stronger Ising interaction strength is needed, which is still challenging experimentally.

V. SUMMARY

In summary, we have studied phase transitions in an Ising chain with transverse field and coupled to a multimode resonator field beyond the long-wavelength approximation. We find that the superradiant phase transition occurs when the coupling between the qubit and resonator field is strong enough, and we show that we can pick a particular field mode to undergo the superradiant phase transition by properly modulating the Ising interaction strength. We further studied the magnetic properties of the Ising chain and discovered a rich set of possible phases by calculating the qubit correlation functions.

ACKNOWLEDGMENTS

This work was funded by National Natural Science Foundation of China (Grant No. 11174270), the National Basic Research Program of China Grants No. 2011CB921204, and No. 2011CBA00200, the Strategic Priority Research Program of the Chinese Academy of Sciences (Grant No. XDB01000000) and Research Fund for the Doctoral Program of Higher Education of China (Grant No. 20103402110024). Z.-W. Zhou gratefully acknowledges the support of the K.C. Wong Education Foundation, Hong Kong.

APPENDIX A: HAMILTONIAN OF CHARGE-QUBIT-CHAIN—TLR SYSTEM

We derive the Hamiltonian for the circuit in Fig. 1 in this section. First, the quantized TLR modes are described by the Hamiltonian ($\hbar = 1$)

$$H_R = \sum_l \omega_l b_l^\dagger b_l, \tag{A1}$$

where $b_l^{(\dagger)}$ is the annihilation (creation) operator for the lth mode, and ω_l is its frequency. ω_l is determined by the physical parameters of the TLR, $\omega_l = l\pi/(d\sqrt{L_0C_0})$, where d is the length of the TLR, and C_0 and L_0 are the capacitance and inductance per unit length. The voltage of the resonator associated with the lth mode can be expressed as $V_l(x) = \sqrt{\frac{\omega_l}{dC_0}}\cos(k_l x)(b_l + b_l^\dagger)$, where $k_l = \omega_l\sqrt{C_0L_0}$ is its wave vector, and $x \in [0,d]$ is the position along the TLR [15].

Now we consider a chain of N equally spaced Cooper-pair boxes embedded in a TLR [15–17], as shown in Fig. 1. Because of the capacitive coupling to the TLR, the total gate voltage for the jth qubit is the sum of a dc bias value and a quantum part due to the TLR voltage. Therefore, the total gate voltage is $V_g(x_j) = V_g^{\rm dc} + \hat{V}(x_j)$, with the quantum part $\hat{V}(x_j) = \sum_l \hat{V}_l(x_j)$. The Hamiltonian for the charge boxes [17] reads

$$H_C = \sum_j \Big\{ 4E_c \sum_n \left(n - n_g^j\right)^2 |n\rangle_j\langle n| - E_z/2 \sum_n (|n+1\rangle_j\langle n| + |n\rangle_j\langle n+1|) \Big\}, \tag{A2}$$

where $E_c = e^2/(2C_\Sigma) = e^2/[2(C_g + C_J)]$ is the charging energy (C_Σ, C_g, and C_J are the total, gate, and Josephson junction capacitance of the charge box, respectively), E_z is the Josephson energy, and $n_g^j = C_g V_g(x_j)/(2e)$ is the excess charge on the jth Cooper pair box. If we bias the charge boxes at the degeneracy point $C_g V_g^{dc}/(2e) = 1/2$, the charge boxes effectively function as two-level qubits with the charge states $n = 0,1$. In this case, the excess charge $n_g^j = 1/2 + C_g\hat{V}(x_j)/(2e)$. In the subspace $\{n = 0,1\}$, the qubit charging energy is

$$\begin{aligned}
&4E_c \sum_j \sum_{n=0,1} \left(n - n_g^j\right)^2 |n\rangle_j\langle n| \\
&= 4E_c \sum_j \sum_{n=0,1} \left[n - \frac{1}{2} - C_g\hat{V}(x_j)/(2e)\right]^2 |n\rangle_j\langle n| \\
&= 4E_c \sum_j \sum_{n=0,1} \left[\left(n - \frac{1}{2}\right)^2 - 2\left(n - \frac{1}{2}\right) C_g\hat{V}(x_j)/(2e) + (C_g\hat{V}(x_j)/(2e))^2\right] |n\rangle_j\langle n| \\
&= \sum_j \left[E_c - 4E_c\frac{C_g\hat{V}(x_j)}{2e}(|1\rangle_j\langle 1| - |0\rangle_j\langle 0|) + 4E_c\frac{C_g^2\hat{V}^2(x_j)}{4e^2}\right],
\end{aligned} \tag{A3}$$

where we have used $|1\rangle_j\langle 1| + |0\rangle_j\langle 0| = 1$. Recall that

$$\hat{V}(x_j) = \sum_l \sqrt{\frac{\omega_l}{dC_0}} \cos(k_l x_j)(b_l + b_l^\dagger). \tag{A4}$$

The second term in Eq. (A3) is the coupling between the TLR and the qubit:

$$H_{Q\text{-}R} = 4E_c \frac{C_g}{2e} \sum_j \sum_l \left[\sqrt{\frac{\omega_l}{dC_0}} \cos(k_l x_j) \right.$$
$$\left. (b_l + b_l^\dagger)(|1\rangle_j\langle 1| - |0\rangle_j\langle 0|) \right]. \tag{A5}$$

The third term gives rise to the self-energy of the TLR:

$$H_{R\text{-}R} = 4E_c \frac{C_g^2}{4e^2} \sum_j \sum_l \frac{\omega_l}{dC_0} \cos^2(k_l x_j)(b_l + b_l^\dagger)^2, \tag{A6}$$

where we have used $\sum_j \cos(k_l x_j)\cos(k_{l'} x_j) \sim 0$ for $l \neq l'$ and ignored the coupling between different resonator modes. The Hamiltonian of the qubits is given by the Josephson energy term in Eq. (A2):

$$H_Q = -\frac{E_z}{2} \sum_j (|1\rangle_j\langle 0| + |0\rangle_j\langle 1|). \tag{A7}$$

In the qubit eigenstates $\{(|0\rangle \pm |1\rangle)/\sqrt{2}\}$, the total Hamiltonian of the system then reads

$$\begin{aligned} H &= H_R + H_Q + H_{Q\text{-}R} + H_{R\text{-}R}, \\ H_Q &= -\frac{E_z}{2} \sum_j \sigma_j^z, \\ H_{Q\text{-}R} &= -\sum_j \sum_l \frac{\lambda_l(j)}{\sqrt{N}} \sigma_j^x (b_l^\dagger + b_l), \\ H_{R\text{-}R} &= \sum_l D_l (b_l + b_l^\dagger)^2, \end{aligned} \tag{A8}$$

where $\lambda_l(j) = \lambda_0 \sqrt{l} \cos(l\pi j/N)$, $D_l = \frac{1}{N}\sum_j \frac{C_\Sigma}{2e^2}\lambda_l^2(j)$, with $\lambda_0 = \frac{eC_g}{C_\Sigma}\sqrt{\frac{N\omega_1}{dC_0}}$.

Furthermore, adjacent charge boxes can be coupled by using an rf superconducting quantum interference device (rf-SQUID) mediated tunable coupler as shown in Fig. 1. The rf-SQUID acts as an inductive transformer leading to an effective mutual inductive energy [28,29]:

$$H_{Q\text{-}Q} = -\sum_j M_{\text{eff}}(j) I_j I_{j+1}, \tag{A9}$$

where $M_{\text{eff}}(j)$ is the effective mutual inductance, and I_j is the total current through the jth junction. For charge qubits, we have $I_j = -\frac{C_g}{2e}\ddot{\varphi}_j$ and $\frac{C_\Sigma}{2e}\ddot{\varphi}_j + I_c \sin(\varphi_j) = 0$, where φ_j is the junction phase, and I_c is the critical current. Then we have $I_j = \frac{C_g}{C_\Sigma} I_c \sin(\varphi_j)$ and

$$\begin{aligned} H_{Q\text{-}Q} &= -\sum_j J(j) \sin(\varphi_j)\sin(\varphi_{j+1}) \\ &= -\sum_j J(j) \sigma_j^y \sigma_{j+1}^y, \end{aligned} \tag{A10}$$

where $J(j) = [M_{\text{eff}}(j) C_g^2 I_c^2]/C_\Sigma^2$, and we have used $\sin(\varphi) = \sigma^y$. It is assumed that the coupler is placed far away from the TLR and the coupling to TLR can be ignored.

In summary, the total Hamiltonian of the system is

$$H = H_R + H_Q + H_{Q\text{-}R} + H_{R\text{-}R} + H_{Q\text{-}Q}, \tag{A11}$$

where each component of the Hamiltonian is given in Eqs. (A8) and (A10).

APPENDIX B: MEAN-FIELD SOLUTION

The Hamiltonian in Eq. (A11) can be solved in the mean-field approximation for the resonator field. For simplicity of presentation, we first consider only one single TLR mode l. Under the mean-field approximation for $H_{Q\text{-}R}$ as in Eq. (8), the total Hamiltonian reads

$$\begin{aligned} H &= \omega_l b_l^\dagger b_l + D_l(b_l^\dagger + b_l)^2 - \sqrt{N}\Sigma_l^x (b_l^\dagger + b_l) \\ &\quad - \sum_j \frac{E_z}{2}\sigma_j^z - \sum_j 2\lambda_l(j)\phi_l \sigma_j^x - \sum_j J(j)\sigma_j^y \sigma_{j+1}^y \\ &\quad + 2N\phi_l \Sigma_l^x, \end{aligned} \tag{B1}$$

where ϕ_l and Σ_l^x are the mean values of the resonator field and qubit chain, respectively. The first line of Eq. (B1) can be diagonalized, and the Hamiltonian then becomes

$$\begin{aligned} H &= \bar{\omega}_l \bar{b}_l^\dagger \bar{b}_l - \frac{N(\Sigma_l^x)^2}{\bar{\omega}_l(\alpha+\beta)^2} - \sum_j \frac{E_z}{2}\sigma_j^z - \sum_j 2\lambda_l(j)\phi_l \sigma_j^x \\ &\quad - \sum_j J(j)\sigma_j^y \sigma_{j+1}^y + 2N\phi_l \Sigma_l^x, \end{aligned} \tag{B2}$$

where $\bar{b}_l = \alpha b_l + \beta b_l^\dagger + \frac{\sqrt{N}\Sigma_l^x}{\bar{\omega}_l(\alpha+\beta)}$ with $\bar{\omega}_l = (\omega_l^2 + 4D_l\omega_l)^{1/2}$, $\alpha = [(\omega_l + 2D_l + \bar{\omega}_l)/(2\omega_l)]^{1/2}$, and $\beta = [(\omega_l + 2D_l - \bar{\omega}_l)/(2\omega_l)]^{1/2}$.

The second line of Eq. (B1) describes a nonlocal Ising chain with nonuniform transverse field. To find its spectrum, we first make a local rotation along the y axis to introduce the Pauli matrices $\bar{\sigma}_j^z = \cos(\theta_j)\sigma_j^z + \sin(\theta_j)\sigma_j^x$, $\bar{\sigma}_j^x = \cos(\theta_j)\sigma_j^x - \sin(\theta_j)\sigma_j^z$, and $\bar{\sigma}_j^y = \sigma_j^y$, with $\theta_j = \arctan\{[4\lambda_l(j)\phi_l]/E_z\}$. Then the second line of Eq. (B1) takes the form

$$H_{\text{Ising}} = -\sum_j \Omega(j)\bar{\sigma}_j^z - \sum_j J(j)\bar{\sigma}_j^y \bar{\sigma}_{j+1}^y, \tag{B3}$$

where the effective transverse magnetic field

$$\Omega(j) = \sqrt{\left(\frac{E_z}{2}\right)^2 + [2\lambda_l(j)\phi_l]^2}. \tag{B4}$$

We assume the periodic boundary condition for the qubit chain, $\bar{\sigma}_{N+1} = \bar{\sigma}_1$. Following the method given in Refs. [30–35], we express the Pauli matrices using the creation and annihilation operators in the spinor space:

$$\bar{\sigma}_j^z = 1 - 2a_j^\dagger a_j, \quad \bar{\sigma}_j^y = a_j^\dagger + a_j, \tag{B5}$$

and apply the Jordan–Wigner transformation

$$a_j^\dagger = c_j^\dagger e^{-i\pi\sum_{i=1}^{j-1} c_i^\dagger c_i}, \quad a_j = e^{-i\pi\sum_{i=1}^{j-1} c_i^\dagger c_i} c_j, \tag{B6}$$

to map the qubit chain to a collection of fermions described by the creation and annihilation operators $c^\dagger$ and c which satisfy $\{c_i,c_j^\dagger\}=\delta_{ij}$ and $\{c_i,c_j\}=\{c_i^\dagger,c_j^\dagger\}=0$. After this transformation, we obtain a quadratic Hamiltonian in fermion operators

$$\begin{aligned} H_{\text{Ising}} &= -\sum_{j=1}^{N}\Omega(j)(1-2c_j^\dagger c_j) \\ &\quad -\sum_{j=1}^{N-1}J(j)(c_j^\dagger-c_j)(c_{j+1}^\dagger+c_{j+1}) \\ &\quad +J_N(c_N^\dagger-c_N)(c_1^\dagger+c_1)e^{i\pi\mathcal{N}} \\ &= \sum_{i,j}c_i^\dagger A_{ij}c_j+\sum_{i,j}(c_i^\dagger B_{ij}c_j^\dagger+c_iB_{ij}c_j), \end{aligned} \tag{B7}$$

where

$$\begin{aligned} &A_{j,j}=\Omega_j,\quad A_{j,j+1}=-\frac{J(j)}{2},\quad A_{j+1,j}=-\frac{J(j)}{2}, \\ &B_{j,j+1}=\frac{J(j)}{2},\quad B_{j+1,j}=-\frac{J(j)}{2}, \\ &A_{N,1}=-\frac{J(N)}{2}e^{i\pi\mathcal{N}},\quad A_{1,N}=-\frac{J(N)}{2}e^{i\pi\mathcal{N}}, \\ &B_{N,1}=\frac{J(N)}{2}e^{i\pi\mathcal{N}},\quad B_{1,N}=-\frac{J(N)}{2}e^{i\pi\mathcal{N}}, \end{aligned} \tag{B8}$$

and $\mathcal{N}=\sum_{j=1}^{N}c_j^\dagger c_j$ is the number of fermions. Although the spin problem has a periodic boundary condition, the transformed fermion problem could have a periodic or antiperiodic boundary condition, depending on the fermion number $\mathcal{N}$. Specifically, the fermion problem has an antiperiodic boundary condition if there is an even number of fermions, and periodic boundary condition if there is an odd number of fermions. The ground state is in the sector with antiperiodic boundary condition [30].

The bilinear Hamiltonian in Eq. (B8) can be diagonalized exactly. To do so, we perform the linear canonical transformation

$$\eta_k=\sum_j(g_{kj}c_j+h_{kj}c_j^\dagger), \tag{B9}$$

$$\eta_k^\dagger=\sum_j(g_{kj}c_j^\dagger+h_{kj}c_j), \tag{B10}$$

where the η_ks are a new set of fermionic quasiparticle operators, $\{\eta_k,\eta_{k'}^\dagger\}=\delta_{kk'}$, $\{\eta_k,\eta_{k'}\}=\{\eta_k^\dagger,\eta_{k'}^\dagger\}=0$, and the coefficients are chosen to be real. In order to diagonalize the Hamiltonian and express it in the form

$$H_{\text{Ising}}=\sum_{k=1}^{N}\Lambda_k\left(\eta_k^\dagger\eta_k-\frac{1}{2}\right), \tag{B11}$$

the coefficients g_{ki} and h_{ki} must satisfy [35]

$$\Lambda_k^2\Phi_{k,j}=\sum_i\Phi_{k,i}(A-B)(A+B)_{i,j}, \tag{B12}$$

$$\Lambda_k^2\Psi_{k,j}=\sum_i\Psi_{k,i}(A+B)(A-B)_{i,j}, \tag{B13}$$

where $\Phi_{k,j}$ and $\Psi_{k,j}$ are linear combinations of g_{ki}, h_{ki},

$$\Phi_{kj}=g_{kj}+h_{kj}, \tag{B14}$$

$$\Psi_{kj}=g_{kj}-h_{kj}. \tag{B15}$$

By solving these equations, we can obtain the quasiparticle spectrum Λ_k and the coefficients g_{ki} and h_{ki}.

The total Hamiltonian then reads

$$H=\bar{\omega}_l\bar{b}_l^\dagger\bar{b}_l-\frac{N\left(\Sigma_l^x\right)^2}{\bar{\omega}_l(\alpha+\beta)^2}+\sum_{k=1}^{N}\Lambda_k\left(\eta_k^\dagger\eta_k-\frac{1}{2}\right)+2N\phi_l\Sigma_l^x. \tag{B16}$$

The ground state $|G\rangle$ must satisfy

$$\bar{b}_l|G\rangle=0,\quad \eta_k|G\rangle=0\ (\forall\ k), \tag{B17}$$

and the ground-state energy is

$$E_g=-\frac{N\left(\Sigma_l^x\right)^2}{\bar{\omega}_l(\alpha+\beta)^2}-\sum_{k=1}^{N}\frac{1}{2}\Lambda_k+2N\phi_l\Sigma_l^x. \tag{B18}$$

From $\bar{b}_l|G\rangle=0$, we get

$$\phi_l=\langle G|\frac{(b_l^\dagger+b_l)}{2\sqrt{N}}|G\rangle=\frac{\Sigma_l^x}{\omega_l+4D_l}, \tag{B19}$$

and therefore

$$E_g=N(\omega_l+4D_l)\phi_l^2-\sum_{k=1}^{N}\frac{1}{2}\Lambda_k. \tag{B20}$$

Notice that $\Omega(j)=[(\frac{E_z}{2})^2+4\lambda_l^2(j)\phi_l^2]^{1/2}$, and Λ_k is also a function of ϕ_l. The value of ϕ_l is determined by minimizing $E_g(\phi_l)$. If $E_g(\phi_l^g)$ is the minimum, we have $\frac{\partial E_g(\phi_l)}{\partial\phi_l}|_{\phi_l^g}=0$. Notice

$$\begin{aligned} -\sum_{k=1}^{N}\frac{1}{2}\Lambda_k &= \langle G|-\sum_j\frac{E_z}{2}\sigma_j^z-\sum_j2\lambda_l(j)\phi_l\sigma_j^x \\ &\quad -\sum_jJ(j)\sigma_j^y\sigma_{j+1}^y|G\rangle, \end{aligned} \tag{B21}$$

and

$$\begin{aligned} &\frac{\partial}{\partial\phi_l}\langle G|\sum_j\frac{E_z}{2}\sigma_j^z-\sum_j2\lambda_l(j)\phi_l\sigma_j^x-\sum_jJ(j)\sigma_j^y\sigma_{j+1}^y|G\rangle \\ &\quad=-\langle G|\sum_j2\lambda_l(j)\sigma_j^x|G\rangle. \end{aligned} \tag{B22}$$

Therefore, the condition $\frac{\partial E_g(\phi_l)}{\partial\phi_l}|_{\phi_l^g}=0$ leads to

$$\Sigma_l^x=\frac{\langle G|\sum_j\lambda_l(j)\sigma_j^x|G\rangle}{N}=\phi_l(\omega_l+4D_l),$$

which is consistent with the result in Eq. (B19).

We can similarly calculate the ground-state energy for multiple field modes in the thermodynamic limit. The total

Hamiltonian is

$$H = \sum_l [\omega_l b_l^\dagger b_l + D_l(b_l^\dagger + b_l)^2 - \sqrt{N}\Sigma_l^x(b_l^\dagger + b_l)] - \sum_j \frac{E_z}{2}\sigma_j^z - \sum_{j,l} 2\lambda_l(j)\phi_l\sigma_j^x - \sum_j J(j)\sigma_j^y\sigma_{j+1}^y + \sum_l \left(2N\phi_l\Sigma_l^x\right), \quad \text{(B23)}$$

and we have $\Sigma_l^x = \phi_l^g(\omega_l + 4D_l)$. The ground-state energy now reads

$$E_g = \sum_l \left[N(\omega_l + 4D_l)\phi_l^2\right] - \sum_{k=1}^N \frac{1}{2}\Lambda_k, \quad \text{(B24)}$$

and Λ_k is the quasiparticle spectrum of Ising chain (B3) with effective transverse magnetic field

$$\Omega(j) = \sqrt{\left(\frac{E_z}{2}\right)^2 + \left[2\sum_l \lambda_l(j)\phi_l\right]^2}. \quad \text{(B25)}$$

The order parameter ϕ_l^g is determined by minimizing $E_g(\phi_1,\phi_2,\dots)$.

APPENDIX C: QUBIT CORRELATION FUNCTION

Now we show how to calculate the correlation functions. The correlation of the qubit chain at ground state can be calculated using the fermionic operators,

$$\rho_{j,j+n} = \langle\bar\sigma_j^y\bar\sigma_{j+n}^y\rangle = \left\langle (c_j^\dagger + c_j)\left[\prod_{i=j}^{j+n-1}(c_i^\dagger + c_i)(c_i^\dagger - c_i)\right](c_{j+n}^\dagger + c_{j+n})\right\rangle. \quad \text{(C1)}$$

If we define

$$C_j = c_j^\dagger + c_j, \quad D_j = c_j^\dagger - c_j, \quad \text{(C2)}$$

then

$$\rho_{j,j+n} = \langle D_j C_{j+1} D_{j+1}\cdots C_{j+n-1}D_{j+n-1}C_{i+n}\rangle. \quad \text{(C3)}$$

This expectation value can be evaluated by Wick's theorem [33,36] which relates it to a sum over products of expectation values of pairs of operators. By making use of the inverse transformation

$$C_j = \sum_k \Phi_{kj}(\eta_k^\dagger + \eta_k), \quad D_j = \sum_k \Psi_{kj}(\eta_k^\dagger - \eta_k), \quad \text{(C4)}$$

and $\eta_k|G\rangle = 0$, the expectation value of any such pair is easily calculated:

$$\begin{aligned}\langle C_i C_j\rangle &= \sum_{k,k'}\Phi_{ki}\Phi_{k'j}\langle(\eta_k^\dagger - \eta_k)(\eta_{k'}^\dagger + \eta_{k'})\rangle = \delta_{i,j},\\ \langle D_i D_j\rangle &= \sum_{k,k'}\Psi_{ki}\Psi_{k'j}\langle(\eta_k^\dagger - \eta_k)(\eta_k^\dagger + \eta_{k'})\rangle = -\delta_{i,j},\\ \langle D_i C_j\rangle &= \sum_{k,k'}\Psi_{ki}\Phi_{k'j}\langle(\eta_k^\dagger - \eta_k)(\eta_{k'}^\dagger + \eta_{k'})\rangle = -(\Psi^\top\Phi)_{ij}.\end{aligned} \quad \text{(C5)}$$

Defining

$$G_{i,j} = \langle D_i C_j\rangle, \quad \text{(C6)}$$

and collecting the terms in the Wick expansion, we find

$$\rho_{j,j+n} = \begin{vmatrix} G_{j,j+1} & G_{j,j+2} & \cdots & G_{j,j+n}\\ G_{j+1,j+1} & G_{j+1,j+2} & \cdots & \vdots\\ \vdots & \vdots & \ddots & \vdots\\ G_{j+n-1,j+1} & G_{j+n-1,j+2} & \cdots & G_{j+n-1,j+n}\end{vmatrix}. \quad \text{(C7)}$$

$\langle\bar\sigma_j^z\rangle$ and $\langle\bar\sigma_j^x\rangle$ can also be calculated in the same way:

$$\langle\bar\sigma_j^z\rangle = (\Psi^\top\Phi)_{j,j}, \quad \langle\bar\sigma_j^x\rangle = 0. \quad \text{(C8)}$$

We can rotate $\bar{\boldsymbol\sigma}$ back to $\boldsymbol\sigma$,

$$\begin{aligned}\langle\sigma_j^y\sigma_{j+n}^y\rangle &= \langle\bar\sigma_j^y\bar\sigma_{j+n}^y\rangle,\\ \langle\sigma_j^z\rangle &= \cos(\theta_j)\langle\bar\sigma_j^z\rangle,\\ \langle\sigma_j^x\rangle &= \sin(\theta_j)\langle\bar\sigma_j^z\rangle.\end{aligned} \quad \text{(C9)}$$

[1] R. P. Feynman, Int. J. Theor. Phys. **21**, 467 (1982).
[2] S. Lloyd, Science **273**, 1073 (1996).
[3] Iulia Buluta and Franco Nori, Science **326**, 108 (2009).
[4] J. I. Cirac and P. Zoller, Nat. Phys. **8**, 264 (2012).
[5] Andrew A. Houck, Hakan E. Tureci, and Jens Koch, Nat. Phys. **8**, 292 (2012).
[6] P. Hauke, F. M. Cucchietti, L. Tagliacozzo, I. Deutsch, and M. Lewenstein, Rep. Prog. Phys. **75**, 082401 (2012).
[7] Y. Makhlin, G. Schön, and A. Shnirman, Rev. Mod. Phys. **73**, 357 (2001).
[8] J. Clarke and F. K. Wilhelm, Nature (London) **453**, 1031 (2008).
[9] S. Mostame, P. Rebentrost, A. Eisfeld, A. J. Kerman, D. I. Tsomokos, and A. Aspuru-Guzik, New J. Phys. **14**, 105013 (2012).
[10] Feng Mei, Vladimir M. Stojanovic, Irfan Siddiqi, and Lin Tian, Phys. Rev. B **88**, 224502 (2013).
[11] Vladimir M. Stojanovic, Mihajlo Vanevic, Eugene Demler, and Lin Tian, Phys. Rev. B **89**, 144508 (2014).
[12] R. H. Dicke, Phys. Rev. **93**, 99 (1954).
[13] K. Hepp and E. H. Lieb, Phys. Rev. A **8**, 2517 (1973).
[14] Y. K. Wang and F. T. Hioe, Phys. Rev. A **7**, 831 (1973).

[15] A. Blais, R. S. Huang, A. Wallraff, S. M. Girvin, and R. J. Schoelkopf, Phys. Rev. A **69**, 062320 (2004).
[16] A. Blais, J. Gambetta, A. Wallraff, D. I. Schuster, S. M. Girvin, M. H. Devoret, and R. J. Schoelkopf, Phys. Rev. A **75**, 032329 (2007).
[17] P. Nataf and C. Ciuti, Nat. Commun. **1**, 72 (2010).
[18] Clive Emary and Tobias Brandes, Phys. Rev. E **67**, 066203 (2003).
[19] C. F. Lee and N. F. Johnson, Phys. Rev. Lett. **93**, 083001 (2004).
[20] Soren Gammelmark and Klaus Molmer, New J. Phys. **13**, 053035 (2011).
[21] Kurt Binder, Rep. Prog. Phys. **50**, 783 (1987).
[22] Michael Plischke and Birger Bergersen, *Equilibrium Statistical Physics* (World Scientific Publishing, Singapore, 2006).
[23] A. Wallraff, D. I. Schuster, A. Blais, L. Frunzio, R.-S. Huang, J. Majer, S. Kumar, S. M. Girvin, and R. J. Schoelkopf, Nature (London) **431**, 162 (2004).
[24] L. H. Du, X. Zhou, Y. J. Han, G. C. Guo, and Z. W. Zhou, Phys. Rev. A **86**, 032302 (2012).
[25] R. J. Schoelkopf and S. M. Girvin, Nature (London) **451**, 664 (2008).
[26] Carsten Hutter, Alexander Shnirman, Yuriy Makhlin, and Gern Schon, Europhys. Lett. **74**, 1088 (2006).
[27] D. V. Averin and C. Bruder, Phys. Rev. Lett. **91**, 057003 (2003).
[28] A. M. van den Brink, A. J. Berkley, and M. Yalowsky, New J. Phys. **7**, 230 (2005).
[29] L. Tian, M. S. Allman, and R. W. Simmonds, New J. Phys. **10**, 115001 (2008).
[30] A. P. Young and H. Rieger, Phys. Rev. B **53**, 8486 (1996).
[31] Oleg Derzhko, J. Phys. A: Math. Gen. **33**, 8627 (2000).
[32] O. Derzhko, J. Richter, T. Krokhmalskii, and O. Zaburannyi, Phys. Rev. E **69**, 066112 (2004).
[33] S. Sachdev, *Quantum Phase Transitions* (Cambridge University Press, Cambridge, 1999).
[34] Jacek Dziarmaga, Phys. Rev. Lett. **95**, 245701 (2005).
[35] E. Lieb, T. Schultz, and D. Mattis, Ann. Phys. (NY) **16**, 407 (1961).
[36] Michael E. Peskin and Daniel V. Schroeder, *An Introduction to Quantum Field Theory* (Westview Press, Reading, MA, 1995).